

The I1 dynein-associated tether and tether head complex is a conserved regulator of ciliary motility

Gang Fu^a, Qian Wang^a, Nhan Phan^a, Paulina Urbanska^b, Ewa Joachimiak^b, Jianfeng Lin^a, Dorota Wloga^b, and Daniela Nicastro^{a,*}

^aDepartments of Cell Biology and Biophysics, University of Texas Southwestern Medical Center, Dallas, TX 75235;

^bLaboratory of Cytoskeleton and Cilia Biology, Department of Cell Biology, Nencki Institute of Experimental Biology of Polish Academy of Sciences, 02-093 Warsaw, Poland

ABSTRACT Motile cilia are essential for propelling cells and moving fluids across tissues. The activity of axonemal dynein motors must be precisely coordinated to generate ciliary motility, but their regulatory mechanisms are not well understood. The tether and tether head (T/TH) complex was hypothesized to provide mechanical feedback during ciliary beating because it links the motor domains of the regulatory I1 dynein to the ciliary doublet microtubule. Combining genetic and biochemical approaches with cryoelectron tomography, we identified FAP44 and FAP43 (plus the algae-specific, FAP43-redundant FAP244) as T/TH components. WT-mutant comparisons revealed that the heterodimeric T/TH complex is required for the positional stability of the I1 dynein motor domains, stable anchoring of CK1 kinase, and proper phosphorylation of the regulatory IC138-subunit. T/TH also interacts with inner dynein arm d and radial spoke 3, another important motility regulator. The T/TH complex is a conserved regulator of I1 dynein and plays an important role in the signaling pathway that is critical for normal ciliary motility.

Monitoring Editor

Wallace Marshall
University of California,
San Francisco

Received: Feb 28, 2018

Accepted: Mar 2, 2018

INTRODUCTION

Cilia and flagella are evolutionarily conserved organelles in eukaryotes ranging from single-celled algae to humans. They play important roles in sensory reception, cell signaling, and motility. Defects or dysfunction of these organelles cause various human diseases,

such as polycystic kidney disease, primary ciliary dyskinesia, hydrocephalus, and infertility (Afzelius, 2004; Fliegauf *et al.*, 2007). The microtubule-based axoneme is the core structure of motile cilia and consists of nine outer doublet microtubules (DMTs) and a central pair complex (CPC). Each DMT is composed of many copies of a 96-nm-long unit that repeats along the length of the axoneme. Two rows of dynein motors, that is, the outer and inner dynein arms (ODAs and IDAs), are bound to each A-tubule of the DMT and drive ciliary beating (Goodenough and Heuser, 1985).

To generate the undulating motion typical of cilia and flagella, the activities of thousands of axonemal dyneins have to be precisely regulated and coordinated (Mitchison and Mitchison, 2010; Kikkawa, 2013). Several complexes have been shown to be involved in the transduction of signals that ultimately regulate the activities of downstream dynein targets. These regulatory complexes include the CPC, the radial spokes, the calmodulin- and radial spoke-associated complex (CSC), the I1 inner arm dynein (or dynein *f*), and the nexin-dynein regulatory complex (N-DRC) (Witman *et al.*, 1978; Smith and Sale, 1992; Smith and Lefebvre, 1997; Smith, 2002; Piperno *et al.*, 1994; Porter and Sale, 2000; Nicastro *et al.*, 2006; Dymeck and Smith, 2007; Bower *et al.*, 2009; Wirschell *et al.*, 2011; Heuser *et al.*, 2012b).

This article was published online ahead of print in MBoC in Press (<http://www.molbiolcell.org/cgi/doi/10.1091/mbc.E18-02-0142>) on March 5, 2018.

Data availability: The three-dimensional averaged structures of the T/TH complex and I1 dynein have been deposited in the Electron Microscopy Data Bank (EMDB) under ID codes EMD-7481, EMD-7486, EMD-7487, EMD-7488, and EMD-7489.

*Address correspondence to: Daniela Nicastro (daniela.nicastro@utsouthwestern.edu).

Abbreviations used: BCCP, biotin carboxyl carrier protein; CPC, central pair complex; cryo-ET, cryoelectron tomography; CSC, calmodulin- and radial spoke-associated complex; DHC, dynein heavy chain; DMT, doublet microtubule; EM, electron microscope; ICLC, intermediate chain and light chain; IDA, inner dynein arm; LC-MS/MS, liquid chromatography–tandem mass spectrometry; MIA, modifier of inner arms; N-DRC, nexin dynein regulatory complex; ODA, outer dynein arm; OID, outer–inner dynein linker; RS, radial spoke; T/TH, tether and tether head.

© 2018 Fu *et al.* This article is distributed by The American Society for Cell Biology under license from the author(s). Two months after publication it is available to the public under an Attribution–Noncommercial–Share Alike 3.0 Unported Creative Commons License (<http://creativecommons.org/licenses/by-nc-sa/3.0>).

“ASCB®,” “The American Society for Cell Biology®,” and “Molecular Biology of the Cell®” are registered trademarks of The American Society for Cell Biology.

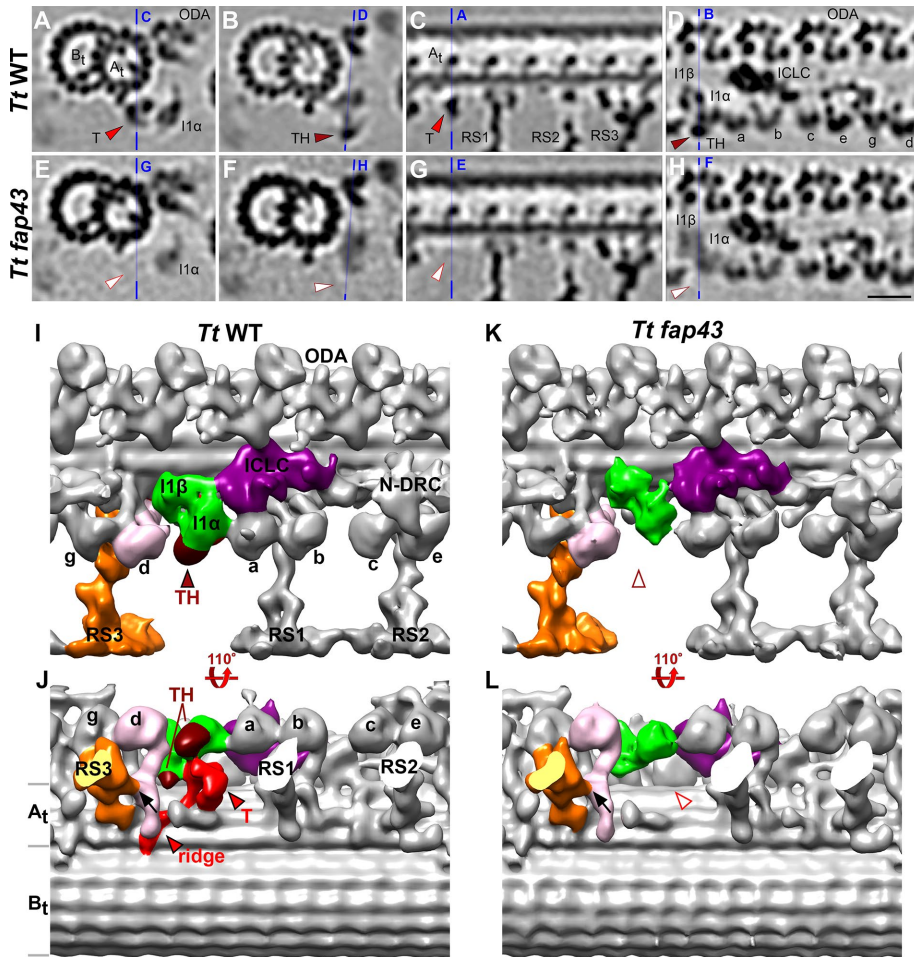


FIGURE 1: Comparison between wild-type and T/TH mutant axonemes to define the three-dimensional structure of the I1-associated T/TH complex. (A–H) Tomographic slices of the averaged 96-nm-long axonemal repeats of wild-type *Tetrahymena thermophila* (A–D) and its *fap43* knockout mutant (E–H) viewed in cross-sectional (A, B, E, and F) and longitudinal (C, D, G, and H) orientations. Note that all cross-sections in the paper are shown viewed from proximal toward the ciliary tip, and in all longitudinal views proximal is on the left, unless otherwise noted. Blue lines indicate the locations of the slices in the respective panels. Electron densities corresponding to tether (T, red arrowheads in A and C) and tether head (TH, dark red arrowheads in B and D) were absent from the *fap43* knockout mutant axonemes (white arrowheads in E–H). (I–L) Isosurface renderings show the three-dimensional structures of the averaged axonemal repeat of wild type and the *fap43* mutant in front (I, K) and bottom (J, L) view. The entire I1 dynein complex (I1 α and I1 β motor domains, green; intermediate and light chain complex (ICLC), purple) was observed in the *fap43* mutant, whereas the tether (red) and tether head (dark red) were completely missing. Black arrows in J and L indicate the connection between inner dynein arm d (IDA d, rose) and radial spoke 3 (RS3, orange). Other labels: A_t and B_t, A- and B-tubule; a–e and g, inner dynein arm isoforms; N-DRC, nexin dynein regulatory complex; ODA, outer dynein arm. Scale bar: 20 nm (valid for A–H).

The I1 dynein is a two-headed IDA containing two dynein heavy chains, I1 α and I1 β , that dimerize through an intermediate chain/light chain complex (ICLC) (Figure 1) (Goodenough and Heuser, 1985; Heuser et al., 2012a). Analyses of flagellar mutants using the model organism *Chlamydomonas reinhardtii* showed that failure of I1 dynein to assemble in the axoneme causes a slow-swimming phenotype and specifically alters the flagellar waveform (reviewed in Wirschell et al., 2007). Previous cryoelectron tomography (cryo-ET) studies revealed the formation of extensive connections between the I1 dynein and its neighboring structures, making it an important regulatory hub within the axonemal 96-nm-long repeat (Heuser et al., 2012a; Yamamoto et al., 2013). Microtubule sliding experi-

ments with I1 mutant flagella demonstrated that hyperphosphorylation of the ICLC-subunit IC138 correlates with slower microtubule sliding, whereas dephosphorylation rescued the sliding activity (Habermacher and Sale, 1997). Thus the I1 dynein complex might exert its regulatory function by altering the phosphorylation state of IC138 (Habermacher and Sale, 1997; Yang and Sale, 2000; Hendrickson et al., 2004). A *Chlamydomonas* mutant lacking the modifier of inner arms (MIA) complex, which when present is connected to the distal end of the I1 ICLC, displayed hyperphosphorylated IC138 and motility defects similar to those of I1 mutants (King and Dutcher, 1997; Yamamoto et al., 2013).

We previously identified another I1-associated structure, the tether and tether head (T/TH) complex that links the I1-dynein motor domains to the ciliary A-tubule (Heuser et al., 2012a). The discovery of this linkage was surprising, because all axonemal dyneins, including the I1 dynein, attach stably to the A-tubule through their cargo-binding tail domains, whereas the motor domains undergo conformational changes that result in the at-least 8-nm-long stepping motion of the dyneins along the B-tubule of the adjacent DMT. Interestingly, a recent structural study of active cilia demonstrated that the T/TH complex undergoes large conformational changes during ciliary beating, and the different states are highly correlated with the direction of ciliary bending (see Supplementary Movie S5 in Lin and Nicastro, 2018). Based on its unique location, connectivity, and dynamics, the T/TH complex was hypothesized to function as regulator and to possibly sense mechanical force caused by the relative motion between the I1 dynein motor domains and the DMTs (Heuser et al., 2012a). However, the unknown protein composition of the T/TH complex and the lack of T/TH mutants have so far prevented functional studies of the T/TH complex.

Here we integrated genetic and biochemical approaches with cryo-ET and identified three flagella-associated proteins, FAP43, FAP44, and FAP244, as components of the T/TH complex. Sequence analyses revealed that FAP43 and FAP44 are conserved proteins, whereas FAP244 is redundant to FAP43 in *Chlamydomonas* but has no homologue in *Tetrahymena* or higher organisms. Comparative proteomics analysis of I1 and here identified T/TH mutants showed that the I1 dynein and the T/TH complex assemble independently of each other. Cryo-ET data revealed the importance of the T/TH complex for stabilizing the I1 dynein motor domains and stable axonemal anchoring of CK1 that phosphorylates the regulatory I1 subunit IC138. Lack of the T/TH complex correlated with misregulation of the phosphorylation status of IC138. These results provide new insights into the composition of the conserved T/TH

complex, its interactions with other axonemal structures, and its functional role in regulating ciliary motility.

RESULTS

FAP43 and FAP44 are T/TH components and are both required for the T/TH complex assembly in *Tetrahymena*

Tetrahymena *gap43* germline knockout mutant cells showed typical ciliary defects, including reduced cell swimming, altered ciliary waveform, proliferation, and phagocytosis rates (Urbanska et al., 2018). Using cryo-ET and subtomogram averaging, we compared the three-dimensional structures of *Tetrahymena* wild-type and *gap43* knockout mutant cilia (Figure 1). In contrast to wild type (Figure 1, A–D, I, and J), the 96 nm axonemal repeats from the *gap43* mutant (Figure 1, E–H, K, and L) lacked the complete T/TH complex, that is, both the tether and tether head structures were missing. All other axonemal components, including the I1 dynein, appeared unaffected in the averaged repeats of *gap43*. This suggests that FAP43 protein is a component of the T/TH complex and required for the complex assembly in the axoneme.

Based on the difference between the wild-type and *gap43* mutant structure, that is, the missing density in *gap43* cilia, the (minimum) size and three-dimensional structure of the T/TH complex could be defined with more precision than before. Previously we observed a tether head (estimated size of 100–150 kDa) attached to the proximal side (AAA6 domain) of the I1 α motor domain and a tether that connected the TH to the ciliary A-tubule (Heuser et al., 2012a). Here we found that a second tether head domain is attached to the proximal side of the I1 β motor domain, and a ridge extends along the bottom of the A-tubule (compare Figure 1, J and L). This confirms the interpretation of the T/TH morphology by a recent study of active cilia (Lin and Nicastro, 2018).

This also means that the size of the T/TH complex is about twice as large as the ~200-kDa FAP43 protein, implying that the T/TH complex contains more than one copy of FAP43 or additional protein components. Thus, we used liquid chromatography–tandem mass spectrometry (LC-MS/MS) to compare *Tetrahymena* wild-type and *gap43* mutant axonemes to probe for potentially additional T/TH subunits. As expected, the mass-spectrometry analysis identified many unique FAP43 peptides in wild-type axonemes but zero in the *gap43* knockout mutant. Interestingly, another ~200-kDa protein, FAP44, was missing specifically from the *gap43* knockout axonemes but not from wild type (Supplemental Table S1), suggesting that FAP44 is also a protein component of the T/TH complex. This agrees well with our coimmunoprecipitation and BirA proximity labeling results that demonstrated a close association between FAP43 and FAP44 in *Tetrahymena* cilia (Urbanska et al., 2018).

In contrast to FAP43 and FAP44, representative I1 dynein proteins were found to be wild-type level in the *gap43* knockout mutant (Supplemental Table S1), indicated that, despite the direct connections between I1 dynein motor domains and the T/TH complex (Heuser et al., 2012a) (Figure 1J), the absence of the T/TH did not affect the assembly of the I1 dynein complex components.

FAP44 but not FAP43 is required for the stable assembly of the T/TH complex in *Chlamydomonas*

The proteomics data identified FAP44 as likely T/TH component (Supplemental Table S1), but a *gap44* mutant was initially unavailable in *Tetrahymena*, for example, to test if FAP44 was required for T/TH assembly. However, based on sequence comparison both FAP43 and FAP44 are highly conserved among ciliated organisms from protists to human (Supplemental Figure S1, A and B). Similarly,

the three-dimensional structure of the T/TH complex also appears highly conserved among ciliated organisms, from protists to human airway cilia (Supplemental Figure S1C). Therefore, we used *Chlamydomonas reinhardtii* as second model organism to study the T/TH complex. We obtained *Chlamydomonas gap43* and *gap44* mutants from the *Chlamydomonas* Library Project (CLiP) (Zhang et al., 2014; Li et al., 2016). To verify the mutations of these CLiP strains, we first confirmed the respective gene disruption by PCR (Urbanska et al., 2018) and then further analyzed their axonemal compositions by comparative LC-MS/MS approach. In all cases, the proteomics results confirmed the complete missing of the corresponding mutated protein from the axonemes (Supplemental Table S1).

Subtomogram averages of the axonemal 96-nm repeats from *Chlamydomonas gap43* and *gap44* mutants were compared with that of wild type (Figure 2). As expected, the entire T/TH complex was missing from the axonemal average of the *Chlamydomonas gap44* mutant (Figure 2, I–L, O, and R), suggesting that FAP44 is required for the stable assembly of the T/TH complex in *Chlamydomonas*, as previously seen for FAP43 in *Tetrahymena*. Surprisingly, however, the average of the 96-nm axonemal repeats from *Chlamydomonas gap43* differed from *Tetrahymena gap43* (Supplemental Figure S2). A classification analysis showed that the majority (86%) of the *Chlamydomonas gap43* axonemal repeats (labeled as *gap43_C1* in Figure 2, E–H, N, and Q) resembled that of wild type with intact T/TH complex (Figure 2, A–D, M, and P and Supplemental Figure S2, I–L), and only 14% of the *Chlamydomonas gap43* repeats lacked the T/TH complex (Supplemental Figure S2, M–P). In contrast to *Tetrahymena gap43* mutant, where FAP43 was required for T/TH assembly, in *Chlamydomonas* FAP43 protein does not seem to be essential for T/TH assembly.

FAP43 and FAP244 are redundant proteins in *Chlamydomonas*, but FAP244 has no homologue in *Tetrahymena*

The above-described discrepancy between the assembly of the T/TH complex in *Tetrahymena* and *Chlamydomonas gap43* mutants raised the possibility that the protein compositions of the T/TH complexes might partly differ in these two organisms. To identify the T/TH protein composition in *Chlamydomonas*, we compared the proteome of *Chlamydomonas* wild-type axonemes to that of the *Chlamydomonas gap44* mutant, which lacked the entire T/TH structure (Figure 2, I–L, O, and R). Similarly to *Tetrahymena*, all known axonemal proteins, including I1 dynein proteins, were present at wild-type levels in the *Chlamydomonas gap44* mutant, with the exception of the mutated protein FAP44 and the T/TH subunit FAP43 (Supplemental Table S1). However, in contrast to *Tetrahymena*, the *Chlamydomonas gap44* mutant lacked in addition FAP244 protein (Supplemental Table S1), indicating that these three proteins are likely components of the *Chlamydomonas* T/TH complex. The BLASTp search revealed FAP244 to be specifically present in green algae species such as *Chlamydomonas* and *Volvox* but to have no homologue in *Tetrahymena* or higher organisms.

The domain architecture of FAP244 is similar to that of FAP43 and FAP44, that is, rich in WD40 repeats at the N-terminal region and coiled-coil domains at the C-terminal region (Supplemental Figure S1A). To investigate the evolutionary relationship between FAP244 and the other two T/TH complex proteins, we constructed a phylogenetic tree with FAP43 and FAP44 sequences from various ciliated organisms (Supplemental Figure S1B). The algorithm sorted the sequences into two clades, the FAP43 and FAP44 clade, respectively, and FAP244 best fits into the FAP43

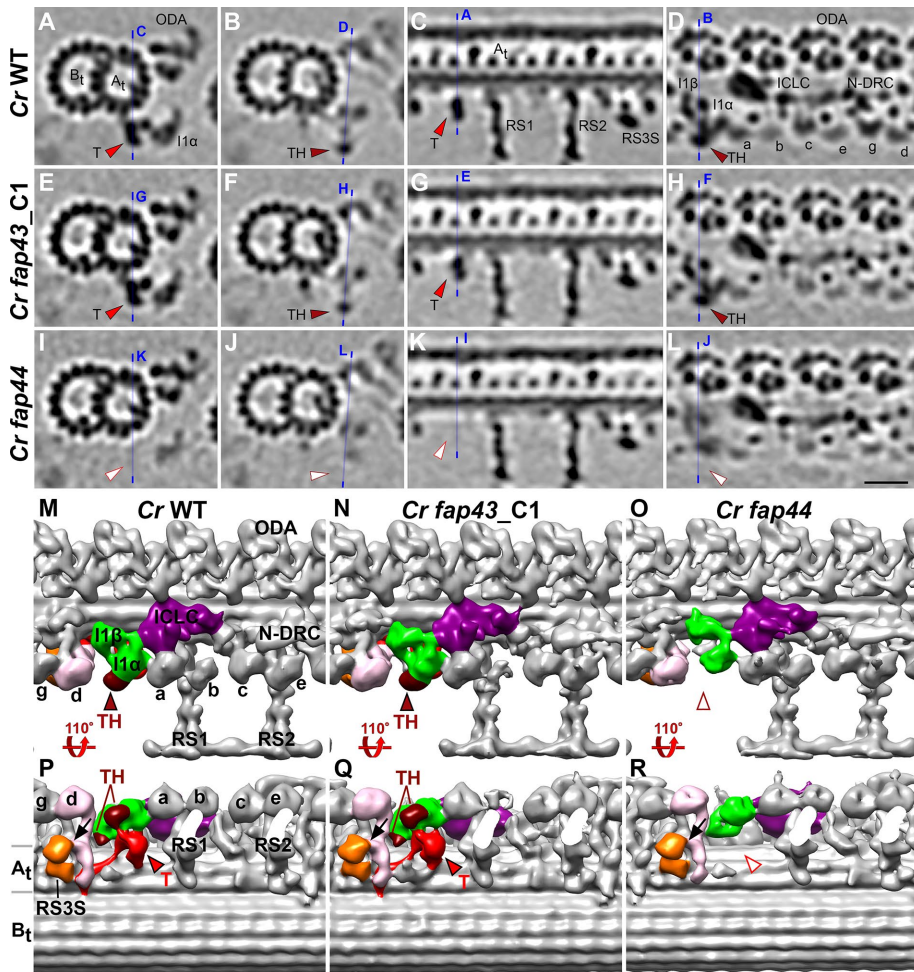


FIGURE 2: FAP44, but not FAP43, is required for the assembly of the T/TH in *Chlamydomonas*. (A–L) Tomographic slices of averaged 96-nm-long axonemal repeats of wild-type *Chlamydomonas reinhardtii* (A–D) and its *fap43* (E–H) and *fap44* (I–L) mutants viewed in cross-sectional (A, B, E, F, I, and J) and longitudinal (C, D, G, H, K, and L) orientations. Blue lines indicate the locations of the slices in the respective panels. Note that *fap43_C1* is a class average containing the majority (86%) of the axonemal repeats from the *fap43* mutant (see also related Supplemental Figure S2 for classification analysis of the T/TH complex in *fap43*). Electron densities corresponding to tether (T, red arrowheads in A, E, G, and I) and tether head (TH, red arrowheads in B, D, F, and H) were observed in wild type and *fap43_C1* but were missing in *fap44* (white arrowheads in I–L). (M–R) Isosurface renderings show the three-dimensional structures of the averaged axonemal repeat of the wild type and *fap43* and *fap44* mutants in front (M, N, and O) and bottom (P, Q, and R) views. Black arrows in P, Q, and R indicate the connection between inner dynein arm d (IDA d, rose) and radial spoke 3 stand-in (RS3S, orange). Other labels: A_t and B_t, A- and B-tubule; a–e and g, inner dynein arm isoforms; ICLC (purple), intermediate and light chain complex; N-DRC, nexin dynein regulatory complex; ODA, outer dynein arm. Scale bar: 20 nm (valid for A–L).

clade. Note that *Chlamydomonas* FAP43 and FAP244 show a close genetic relationship and likely evolved from a duplication event.

To further characterize the T/TH protein composition and possible compositional changes in the *Chlamydomonas* T/TH mutants, we also performed a comparative proteomics analysis using LC-MS/MS of the *Chlamydomonas fap43* and *fap244* mutant axonemes (Supplemental Table S1). Compared to wild type, the amount of FAP44 protein was only slightly reduced in both the *fap43* and *fap244* mutants (in *fap43* somewhat more reduced than in *fap244*). As expected, in the *fap43* and *fap244* mutant axonemes no peptide for the corresponding mutated protein, that is, FAP43 and FAP244,

respectively, were identified, whereas all other known axonemal proteins were present, meaning in *fap43* axonemes FAP244, and in *fap244* axonemes FAP43, protein was still present at wild-type or even higher than wild-type level (Supplemental Table S1), suggesting that FAP43 and FAP244 have (partly) redundant location and function in the axoneme.

Subtomogram averaging combined with classification analysis of the *Chlamydomonas fap244* axonemal repeats resembles the results for *fap43* axonemes, that is, the T/TH complex was absent in only ~10% of the *fap244* axonemal repeats (Supplemental Figure S3), and no additional structural defects were observed. After classification, we analyze the location of the ~10% axonemal repeats that were missing the T/TH complex, but the distribution patterns appeared random, that is, the repeats were neither associated with particular doublet microtubules nor showed any preference to the proximal or distal region along the axoneme length. Taken together, the above results show that in *Chlamydomonas* absence of either FAP43 or FAP244 does not significantly affect the assembly of the T/TH complex and might result in up-regulated expression of the other protein, suggesting that FAP43 or FAP244 are redundant in *Chlamydomonas*.

The ridge of the T/TH complex extends along the A-tubule and interacts with the tail of IDA d

The part of the T/TH complex that is directly attached to the ciliary A-tubule forms a ridge-like structure. The comparison between wild-type cilia of both *Tetrahymena* and *Chlamydomonas* with mutants that lacked the entire T/TH complex, that is, *T.t. fap43* and *C.r. fap44*, showed that the T/TH ridge extends farther than previously reported. Specifically the ridge spans three A-tubule protofilaments (A2–4) all the way to the inner junction between A- and B-tubule (Figures 1J, 2, P and Q, and 3B). In fact, cross-sectional views of the averaged doublet microtubule in the region of the ridge revealed an obvious gap between the tail domain of inner dynein arm d (IDA d) and the surface of the A-tubule protofilaments A2/3 in both mutants (white arrows in Figure 3, D and F) but not wild-type axonemes (red arrows in Figure 3, C and E). Despite this direct interaction between the T/TH ridge and the tail of IDA d in wild type, the stable docking of IDA d to the axoneme was not obviously affected in the T/TH-lacking mutants (Figure 3, C–F). This retention of stability was probably due to additional connections between IDA d and neighboring structures, such as the base of radial spoke 3 (RS3) (black arrows in Figures 1, J and L, and 2, P–R).

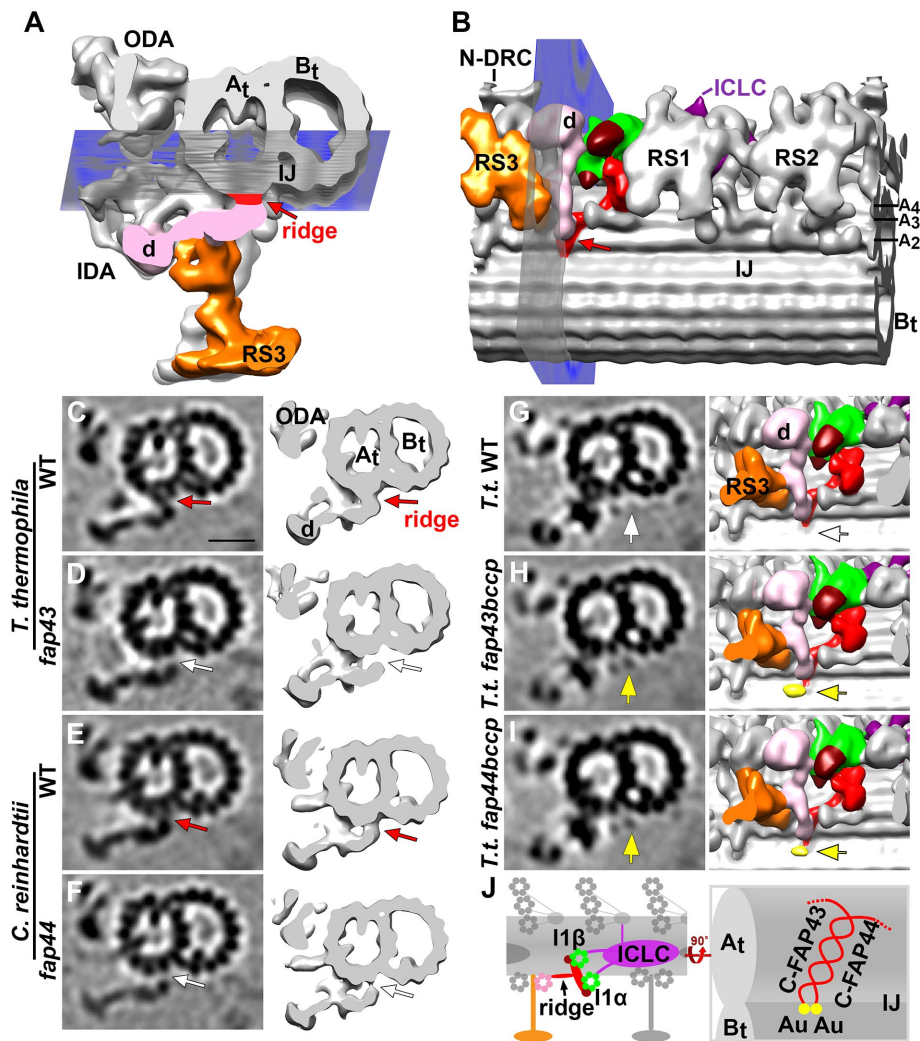


FIGURE 3: Structural characterizations of the T/TH ridge and localization of the C-terminal domains of FAP43 and FAP44 to the ridge. (A, B) Isosurface rendering in cross-sectional (A) and bottom (B) views of the averaged axonemal repeats from wild-type *Tetrahymena*. Note that in this figure all cross-sections are viewed from the ciliary tip toward the cell body for an unobstructed view of the ridge density (red arrows). Blue planes in A and B indicate the locations viewed in bottom views (B, G–I) and cross-sections (C–I), respectively. The T/TH ridge (red arrows) extends from protofilament A2 near the inner junction between the A- and B-tubule (A_t, B_t) to A4 (also see Supplemental Figure S4, A and C). (C–F) Cross-sectional tomographic slices (left) and three-dimensional isosurface renderings (right) reveal an interaction of the T/TH ridge with the tail of inner dynein arm d (IDA d) in wild type of *T. thermophila* and *C. reinhardtii* and a gap between IDA d tail and the A-tubule (white arrows) in *T. thermophila fap43* (D) and *C. reinhardtii fap44* (F). (G–I) Comparisons of tomographic slices (left, in cross view) and three-dimensional isosurface renderings (right, in bottom view as shown in B) among the averaged axonemal repeats from *T. thermophila* wild type (G), *fap43bccp* (H), and *fap44bccp* (I) to show the location of the C-termini of FAP43 and FAP44; note that the extra density corresponding to the BCCP-streptavidin-gold label (yellow arrows and isosurface coloring in H and I) was not observed in wild type (white arrows in G) or control samples (Supplemental Figure S4, E and F). (J) Schematic drawing of the tether (red) and tetherhead (dark red) complex and I1 dynein (I1 α and I1 β motor domains, green; ICLC complex, purple) in the longitudinal direction (left) and magnified bottom view (right); FAP43 and FAP44 are predicted to interact with each other through their C-terminal ridge-forming coiled-coil domains; yellow dots indicate the location of the gold (Au) labels in *fap43bccp* and *fap44bccp* (compare to H and I). Other labels: ICLC (purple), intermediate and light chain complex; N-DRC, nexin dynein regulatory complex; ODA, outer dynein arm; RS, radial spoke (RS3 is orange colored). Scale bar: 20 nm (valid for EM images in C–I).

The C-termini of FAP43 and FAP44 are in close proximity to each other at the IJ-end of the T/TH ridge

To investigate the spatial arrangement of the T/TH components FAP43 and FAP44, we generated two *Tetrahymena* strains expressing C-terminally tagged FAP43-BCCP and FAP44-BCCP (biotin carboxyl carrier protein), respectively (Oda and Kikkawa, 2013). After axoneme isolation the tag was made electron microscope (EM) visible by adding biotin and streptavidin-1.4 nm gold (Song *et al.*, 2015).

Compared to the averaged structure of wild-type axonemes (Figure 3G) and control axonemes (with BCCP tag but without adding streptavidin-gold; Supplemental Figure S4, E and F), an additional density corresponding to the tag with streptavidin-gold was observed at the end of the T/TH ridge close to the inner A/B junction in both *fap43bccp* (yellow arrows in Figure 3H) and *fap44bccp* axonemes (yellow arrows in Figure 3I). Thus, the labeling experiment revealed that the C-termini of both FAP43 and FAP44 are located at nearly the same position in *Tetrahymena*. The enrichment of coiled-coil domains in the C-terminal regions of both proteins (Supplemental Figure S1A) suggests that the two proteins may interact with each other through their coiled-coil domains, forming a heterodimer complex. These results are consistent with the observation that C-terminal fragments of both FAP43 and FAP44 are required and sufficient for ciliary localization, whereas N-terminal fragments remained in the cell body (Urbanska *et al.*, 2018).

The T/TH complex is important for the structural/positional stability of I1 dynein motor domains

Subtomogram averaging of repetitive structures is a powerful method for increasing the signal-to-noise ratio and thus the resolution of molecular details in inherently noisy cryotomograms of native cellular structures (Nicastro *et al.*, 2006). However, if structures are only partially present or positionally flexible, then the averaged electron density of the structure is weakened and blurred. These effects were observed for the electron densities of both I1 dynein motor domains in the T/TH-lacking mutants (Figure 4), *T.t. fap43* (Figure 4B) and *C.r. fap44* (Figure 4G), as compared with the corresponding wild-type structures (*T.t.*: Figure 4A and *C.r.*: Figure 4F). Therefore, we applied an automatic image classification

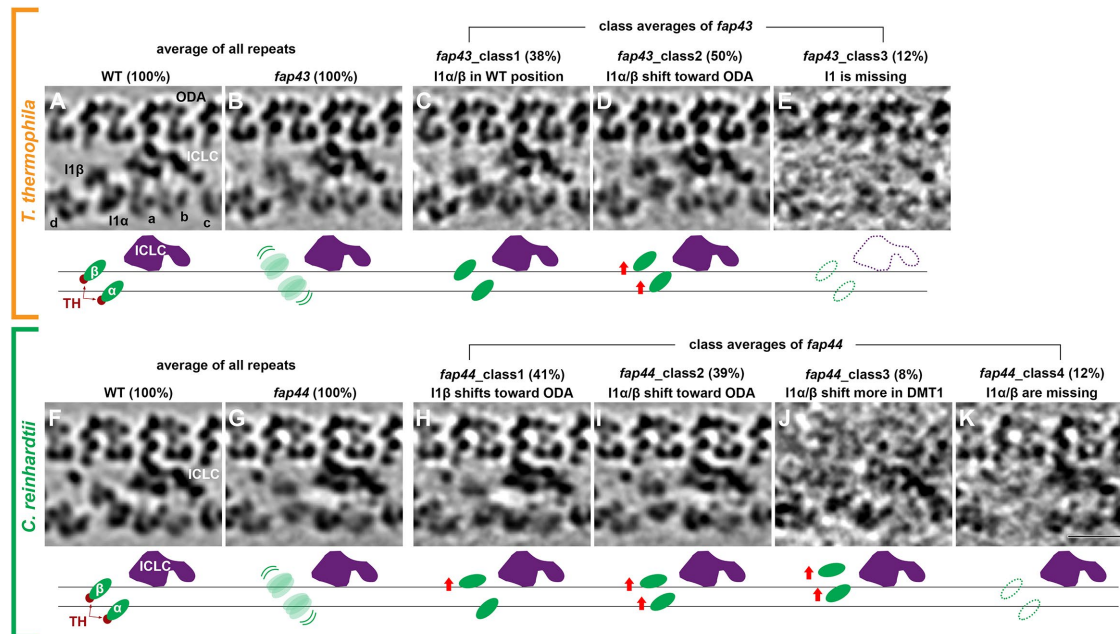


FIGURE 4: Classification analyses reveal importance of T/TH complex for the structural/positional stability of the I1 dynein motor domains. (A–K) Tomographic slices (top) and schematic drawings (bottom) show the averages from all axonemal repeats (100%) from *T. thermophila* wild type (WT, A) and its *fap43* mutant (B), as well as in *C. reinhardtii* wild type (WT, F) and its *fap44* mutant (G). Note the relative weak and blurry appearance of the I1 α and I1 β motor domain densities in *T.t. fap43* (B) and *C.r. fap44* (G). Classification analyses focused on the I1 dynein motors of the axonemal repeats from *T.t. fap43* (C–E) and *C.r. fap44* (H–K) resulted in three and four classes, respectively. The key structural differences and the percentages of repeats included in each class are indicated. The horizontal black lines in the schematic drawings indicate the wild-type positions of the I1 α / β motor domains (green). Other labels: a–d, inner dynein arm isoforms; ICLC (purple), intermediate and light chain complex; ODA, outer dynein arm. Scale bar: 20 nm.

analysis (Heumann *et al.*, 2011) with different masks covering all but the structure of interest, for example, to focus the classification on the dynein motor domains and to separate axonemal repeats with structural differences into homogeneous class averages.

Classification of wild-type repeats for both organisms showed only one structurally homogenous class with 100% of the axonemal repeats (Figure 4, A and F; please note that doublet #1 from *Chlamydomonas* proximal region tomograms was excluded from analysis of both the wild-type and mutant data, because this doublet is known to lack ODAs and I1 dynein [Lin *et al.*, 2012]). In contrast, based on the structural features of the I1 dynein motor domains, the axonemal repeats of *Tetrahymena fap43* and *Chlamydomonas fap44* mutants were grouped into three classes (Figure 4, C–E) and four classes (Figure 4, H–K), respectively. In *Tetrahymena fap43*, 38% of the repeats resembled wild type (class 1, Figure 4C), whereas 50% of the repeats had the I1 motor domains positioned closer to the row of ODAs (class 2, Figure 4D). In the remaining 12% the entire I1 dynein complex was missing (class 3, Figure 4E). In *Chlamydomonas fap44*, one or both of the I1 dynein motors were shifted to different extents closer to the ODA, that is, 41% of the repeats had only I1 β shifted up (class 1, Figure 4H), 39% had both I1 α and I1 β shifted toward the ODAs similar to class 2 of *Tetrahymena fap43* (class 2, Figure 4I), and 8% showed an even greater shift up (class 3, Figure 4J). In the remaining 12% the I1 dynein motor domains—but not the ICLC—were missing (class 4, Figure 4K). Taking the results together, the classification analyses of T/TH-lacking mutants revealed that the T/TH complex plays an important role in stabilizing the position and assembly of the I1 dynein motor domains.

Assembly of the T/TH complex is independent of the I1 dynein complex

To determine whether the assembly of the I1 dynein complex also affects the assembly of the T/TH complex, we investigated the axonemal proteome of the *Chlamydomonas pf9-3* mutant, a *dhc1* mutant that lacks the entire I1 dynein complex (Myser *et al.*, 1997, 1999; Heuser *et al.*, 2012a). As expected all I1 dynein subunits were completely missing or greatly reduced in *pf9-3* (Supplemental Table S1). In contrast, all three *Chlamydomonas* T/TH complex proteins FAP43, FAP44, and FAP244 were present in the mutant at wild-type level (Supplemental Table S1). These results indicated that the T/TH complex was assembled into the axonemal repeat even in the absence of the I1 dynein complex. A previous cryo-ET study of *pf9-3* axonemes reported that the tether heads could not be observed, and the tether density was reduced in the averaged axonemal repeats (Heuser *et al.*, 2012a). In light of our mass-spectrometry data, this suggests that without the connection to the I1 dynein motor domains the T/TH complex is structurally more flexible, causing weakening of the averaged structure, but the docking to the A-tubule is sufficient for stable assembly into the axoneme.

In a T/TH-lacking mutant, IC138 is hyperphosphorylated and CK1 reduced

The I1 dynein complex plays a key role in controlling ciliary motility and the IC138 phosphorylation level seems to be closely associated with the functional state of I1 dynein; for example, IC138 was hyperphosphorylated in paralyzed flagella mutants lacking radial spoke and central pair components, as well as in *mia1* and *mia2* mutants with defective MIA complex that usually binds to the distal region of

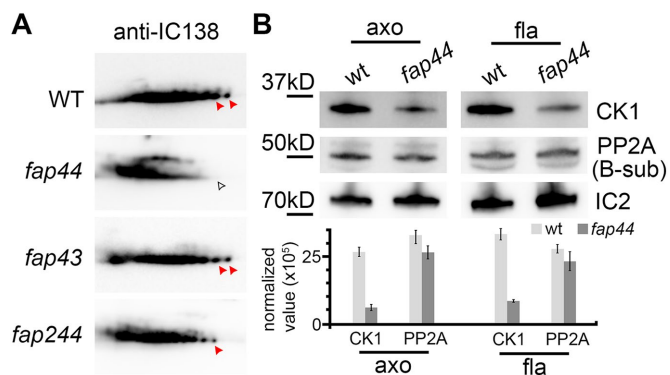


FIGURE 5: Biochemical studies show IC138 hyperphosphorylation and CK1 reduction in the *C. reinhardtii* *fap44* mutant. (A) Two-dimensional gel immunoblots of axonemal proteins extracted from *Chlamydomonas* wild type and *fap44*, *fap43*, and *fap244* mutants probed with anti-IC138. The phosphorylation level of IC138 is higher on the acidic side of the gel (left side) than the basic side (King and Dutcher, 1997). Red arrowheads indicate non- or low-phosphorylated isoforms of IC138, which were reduced in *fap44* (white arrowhead). (B) Immunoblots (top) of axonemal (axo) and flagellar (fla) proteins extracted from *Chlamydomonas* wild type and *fap44*, and relative densitometry quantification of the bands (bottom) normalized to IC2 show reduced abundance of casein kinase 1 (CK1) but not of phosphatase 2A (PP2A) in *fap44*. Blots were probed with anti-CK1, anti-PP2A (B-subunit), and anti-IC2 (control). Results represent mean \pm SD ($n = 3$).

the I1 dynein ICLC (King and Dutcher, 1997; Hendrickson et al., 2004; Yamamoto et al., 2013). Casein kinase I (CK1) and protein phosphatase 2A (PP2A), which are stably anchored to the axoneme, are thought to reversibly phosphorylate and dephosphorylate IC138, respectively (Gokhale et al., 2009; Elam et al., 2011), although direct interactions have not been shown so far. Surprisingly, both CK1 and PP2A were shown to be present at wild-type levels in *Chlamydomonas* mutants that lack the entire I1 dynein (Gokhale et al., 2009). Because of the importance of IC138 as regulatory phospho-switch, we used biochemical methods to test whether the absence of the T/TH complex would be associated with an altered phosphorylation level of IC138 and/or affect CK1 and PP2A abundance.

For better visualization of posttranslational modification, we separated the axonemal proteins from *Chlamydomonas* wild type and the T/TH mutants *fap43*, *fap44*, and *fap244* by two-dimensional gel electrophoresis (2DE) and then performed a Western blot analysis of IC138. Multiple isoforms of IC138 with pI-levels ranging from the acidic to the basic due to different phosphorylation levels were detected (Figure 5A). However, only in the T/TH-lacking *fap44* mutant were more isoforms of IC138 shifted to the acidic side, that is, IC138 was hyperphosphorylated, whereas the IC138 isoforms in wild-type, *fap43*, and *fap244* axonemes showed a similarly uniform distribution across the pH gradient of the gel (Figure 5A) (compare also to King and Dutcher [1997] and Lin and Nicastro [2018]). The results show a correlation between the absence of the T/TH complex and IC138 hyperphosphorylation, indicating that the T/TH complex could be involved in the phosphoregulation signaling cascades that modulate ciliary beating through I1 dynein.

In addition, we tested axonemal and flagellar samples from *Chlamydomonas* wild type and *fap44* with anti-CK1 and anti-PP2A antibodies. Intriguingly, the immunoblots revealed that CK1 was reduced in the mutant, whereas PP2A was assembled at the wild-type level (Figure 5B), suggesting that the T/TH complex is important for stable anchoring of CK1 to the axoneme.

T/TH mutations affect the assembly of a tether-associated base

In addition to the tether ridge that is present in all wild-type axonemal repeats (Supplemental Figure S5, A–C), we observed a second density, here termed “tether-associated base” (Tb, pink density in Supplemental Figure S5A). The latter density is also attached to the A-tubule surface, parallel to the ridge, and connects to the part of the tether that undergoes large conformational motions in active flagella (Lin and Nicastro, 2018). Depending on the image resolution, sometimes only the end-lobe of the tether-associated base close to the inner A/B-junction was visible (Supplemental Figure S5; see Supplemental Table S2 for resolution information). Classification analyses showed species-specific differences in that in *Tetrahymena* wild type all repeats contained the tether-associated base compared with only about half of the axonemal repeats in *Chlamydomonas* wild type (Supplemental Figure S5, B and C) and the I1 dynein-missing mutant *ida2-7* (Supplemental Figure S5, J and K), indicating that the assembly of the tether base was independent of the I1 dynein complex. Moreover, the tether-associated base structure was not observed in axonemes of higher organisms such as sea urchin and humans (Supplemental Figure S1C) (see also Lin et al., 2014).

Interestingly, presence of the T/TH complex had opposite effects on the presence of the tether-associated base in *Chlamydomonas* versus *Tetrahymena*. In the *Chlamydomonas* T/TH mutants *C.r. fap44* (Supplemental Figure S5, D–F) and *C.r. fap43* and *C.r. fap244* (Supplemental Figure S5, L–O), the number of repeats with tether-associated base increased from ~50% to ~70–80%, whereas in *T.t. fap43* the number decreased from 100% to only 75% (Supplemental Figure S5, G–I). The increased occupancy with tether-associated base in *Chlamydomonas* axonemes that lacked the T/TH complex completely (*fap44*) or partially (*fap43* and *fap244*) may point at steric hindrance between the complexes or changed affinity as they assemble into the axoneme. The presence of the tether-associated base in axonemes of some ciliated organisms but not others suggested that the structure may have species-specific characteristics with respect to its assembly and/or function in ciliary motility.

DISCUSSION

Identification of the protein components of the T/TH complex

Cilia are conserved and complex organelles with >650 proteins (Pazour et al., 2005). However, more than half of these proteins have not yet been assigned to a specific ciliary structure (Viswanadha et al., 2017). Thus, locating ciliary proteins within the axoneme and visualizing their native structures at high resolution in situ is crucial for a better understanding of ciliary motility. In this study, through structural and proteomics comparisons between wild type and mutants of a few model organisms, we identified FAP43 and FAP44 to be protein components of the T/TH complex (Table 1). FAP43 and FAP44 were shown to be highly conserved and to have similar domain organizations among ciliated organisms (Supplemental Figure S1, A and B). The evolutionary conservation was not surprising, because previous cryo-ET studies demonstrated very similar three-dimensional morphologies of the T/TH complex in diverse organisms, from single-celled algae to humans (Supplemental Figure S1C) (Lin et al., 2014).

The algae-specific FAP244 was found to be a third T/TH component in *Chlamydomonas*, where it showed some but not fully functional redundancy with FAP43. Although the T/TH complex was largely assembled in both the *C.r. fap43* and *C.r. fap244* axonemes,

Component	Strains					
	<i>T.t.</i> WT	<i>T.t.</i> <i>fap43</i>	<i>C.r.</i> WT	<i>C.r.</i> <i>fap44</i>	<i>C.r.</i> <i>fap43</i>	<i>C.r.</i> <i>fap244</i>
Protein						
FAP43	+	–	+	–	–	+/+
FAP44	+	–	+	–	+/-	+/-
FAP244	N/A	N/A	+	–	+/+	–
Structure						
T/TH complex	+	–	+	–	+/-	+/-
Tb	+	+/-	+	+/+	+/+	+/+

+ indicates that the component was present at wild-type levels; – indicates that the component was absent; +/- indicates that the component was present at reduced levels; +/+ indicates that the component was present at greater than wild-type levels. Tb, tether-associated base.

TABLE 1: Summary of protein and structural components present or absent in T/TH mutants.

the swimming speed of *C.r. fap43* was significantly reduced—similarly to that of the T/TH-lacking *C.r. fap44* and *T.t. fap43* mutants—whereas *fap244* cells swam with wild-type speed (Urbanska *et al.*, 2018), suggesting FAP43 to be more critical than FAP244 to the proper function of the T/TH complex.

FAP43 and FAP44 dimerize and anchor to the axoneme through their C-terminal coiled-coil domains

Several lines of evidence suggest that FAP43 and FAP44 form a heterodimer complex in *Tetrahymena* and higher ciliated organisms through interactions of their C-terminal coiled-coil domains, and this dimerization domain is required and sufficient for anchoring of the T/TH complex to the axoneme. The BCCP-gold labeling revealed that the C-termini of FAP43 and FAP44 were located in close proximity to each other near the inner A/B junction (Figure 3, H–J). In addition, BirA proximity labeling and co-IP experiments demonstrated close proximity (<10 nm) and interactions between FAP43 and FAP44 (Urbanska *et al.*, 2018). Germline knockout of the *fap43* gene and somatic knockout of the *fap44* gene in *Tetrahymena* (Urbanska *et al.*, 2018), as well as disruption of the *fap44* gene in *Chlamydomonas*, resulted in a failure of the T/TH complex to stably assemble into the axoneme. Furthermore, the C-terminal fragments of FAP43 or FAP44 were shown to be necessary and sufficient for ciliary localization in *Tetrahymena*, whereas the WD-repeat-rich N-terminal fragments accumulated in the cell body (Urbanska *et al.*, 2018). This suggests interdependence between the C-terminal domains of FAP43 and FAP44 for T/TH assembly and complex docking to the axoneme.

Structural characterizations of the T/TH complex

By identifying T/TH mutants, specifically *T.t. fap43* and *C.r. fap44*, that lack the entire T/TH complex, we were able to unambiguously characterize the structural details of the T/TH complex and to arrive at several findings: 1) in contrast to only one previously described tether head (Heuser *et al.*, 2012a), we found two tether head domains, one attached to each I1 dynein motor, that is, I1 α and I1 β (Figures 1J, 2, P and Q and 6A). 2) The tether displayed a starlike morphology with four-to-five connections to surrounding axonemal structures (Supplemental Figure S5A); that is, via the tether heads to the I1 motor domains I1 α and I1 β and via the elongated tether ridge to the A-tubule anchoring site and to the tail of IDA d. The ridge, which is likely formed by the C-termini of FAP43 and FAP44, might also in a suitable position to interact with other axonemal structures, such as the base of radial spoke 3. The latter is the location of the CSC, another important regulator for ciliary motility (Dymek and Smith, 2007; Dymek *et al.*, 2011; Heuser *et al.*, 2012b; Urbanska

et al., 2015). The A-tubule interaction through the tether-associated base appears less evolutionarily conserved.

Function(s) of the T/TH complex

All T/TH mutant cells (except for *C.r. fap244*) exhibited reduced swimming velocity and altered ciliary waveform phenotypes (Urbanska *et al.*, 2018), which resembled those of I1 dynein mutants (Wirschell *et al.*, 2007). In T/TH-lacking mutants, the I1 dynein motor domains were positionally destabilized, IC138 was hyperphosphorylated, and CK1 was reduced (Figure 6B), which has previously been correlated to an inactive state of I1 dynein based on microtubule sliding assays (Habermacher and Sale, 1997; Yang and Sale, 2000; Hendrickson *et al.*, 2004). Together this suggests that the T/TH complex is an I1 dynein regulator and thus could be a “missing link” within the CPC-RS-I1 regulatory pathway, which is critical for proper ciliary motility (Figure 6A) (Porter and Sale, 2000; Kamiya and Yagi, 2014; Viswanadha *et al.*, 2017). In fact, the T/TH complex forms a physically link from the tail of dynein d and possibly the base of RS3 through the tether ridge and the tether that transiently connects to the ICLC in active cilia (Lin and Nicastro, 2018) and to the tether heads that directly attach to the I1 dynein motors.

IC138 hyperphosphorylation has been reported previously for other I1-related mutants with defects in the I1 ICLC (Bower *et al.*, 2009; Wirschell *et al.*, 2009; VanderWaal *et al.*, 2011) or the ICLC-associated MIA complex (Yamamoto *et al.*, 2013), but the direct cause of the changed phosphorylation level has not been identified. Similarly, it is not clear what caused the IC138 hyperphosphorylation in *C.r. fap44*, especially as the CK1 level was reduced in this mutant. However, it is possible that lack of the T/TH complex could result in mis-regulation of the remaining CK1 or other kinases and phosphatases targeting IC138. The unique location of the T/TH complex suggests that it could regulate the phosphorylation level of IC138 and/or the I1 dynein activity state through a different mechanism(s) than other I1-regulators (Figure 6):

- 1) The T/TH complex could regulate the I1 dynein activity state through the tether head connection to the I1 motor domains. Of the two dynein heavy chains, I1 β showed the more severe structural phenotype in the *C.r. fap44* mutant—which also showed abnormal phosphorylation level of IC138—as the motor domain was shifted or missing in all axonemal repeats (Figure 4, H–K). This is consistent with previous findings that lack of the I1 β but not the I1 α motor domain is associated with IC138 hyperphosphorylation and defective microtubule sliding (Toba *et al.*, 2011; Lin and Nicastro, 2018).

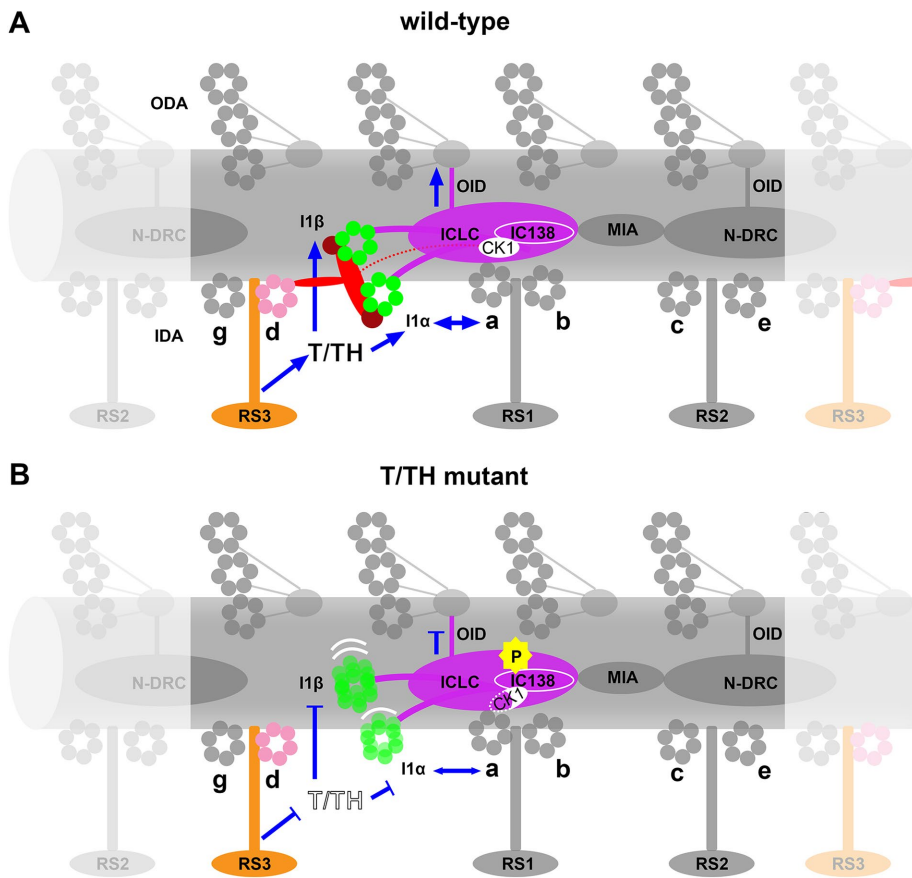


FIGURE 6: Schematic model to summarize the structural features and potential functions of the T/TH complex. (A) In wild-type cilia, the tether head (TH, dark red) binds to the I1 dynein motor domains I1 α and I1 β (green), and the tether (T, red) connects the tether head to the A-tubule through the anchoring ridge structure. Structurally the T/TH complex links several major axonemal complexes; blue arrows indicate potential (direct) signaling pathways between the T/TH complex and these axonemal structures that are involved in regulating ciliary motility. The dotted red line indicates a transient connection between the T/TH and the I1 intermediate chain light chain complex (ICLC, purple) that is only visible in specific regions of actively beating cilia (Lin and Nicastro, 2018). (B) Failure to assemble the T/TH complex in mutants may cause interruption (blocked blue lines) of signal transduction through the T/TH complex from/to the following complexes: radial spoke 3 (RS3, orange), inner dynein arm d (IDA d, rose), the I1 α and I1 β dynein motor domains, and the I1 ICLC, as well as indirectly the other dynein arms (ODA), IDA a and the nexin dynein regulatory complex (N-DRC). The T/TH complex seems also involved in proper function of the kinase/phosphatase, indicated by the hyperphosphorylation (P) of IC138 and reduction of CK1. Together, loss of the T/TH complex resulted in impaired ciliary motility.

2) The CPC-RS-I1 phosphoregulation pathway also includes a network of kinases and phosphatases, including but not limited to CK1 and PP2A. CK1, which is required for proper regulation of microtubule sliding, is distributed along the length of axonemes (Yang and Sale, 2000; Gokhale *et al.*, 2009) and predicted to be located in close proximity to its possible substrate IC138. However, the mechanism for targeting and anchoring CK1 within axoneme is not well understood (reviewed in Wirschell *et al.*, 2011). On the basis of our finding that the T/TH complex and CK1 likely interact (Figure 5B), we propose that CK1 might be “sandwiched” between the tether and the I1 ICLC (on the A-tubule facing side of the ICLC). In a recent cryo-ET study of active flagella, we observed an additional connection between the tether and the I1 ICLC (on the A-tubule-facing side) that seemed transient and only visible in specific regions of actively beating cilia

(Lin and Nicastro, 2018). If CK1 would bind to the tether at or close to this transient tether-ICLC connection, then this could explain why CK1 is still present in *Chlamydomonas* mutants missing the I1 dynein or the MIA complex (Gokhale *et al.*, 2009; Yamamoto *et al.*, 2013), as it could still be bound to the present tether, and why CK1 is only reduced in T/TH-lacking mutants, that is, some CK1 might still bind to the ICLC but with lower affinity than to the tether or transiently during its enzymatic reaction with IC138 or other targets. In fact, the tether might not only serve as stabilizing anchor for CK1 (Figure 6A), but also the large spatial changes that the tether undergoes during ciliary beating (Lin and Nicastro, 2018) might physically coordinate direct interactions between CK1 and IC138/other targets or modulate CK1 activity to ultimately generate the bend-direction specific pattern of dynein activation that underlies ciliary motility.

3) The study of active cilia also revealed bend-direction dependent, transient interactions between the I1 dynein and the N-DRC (through the stalks and microtubule binding domains of I1 dynein), which might allow for signal feedback or cross-talk between these major regulatory hubs (Lin and Nicastro, 2018). Previous cryo-ET studies also revealed connections between the N-DRC and RS3/CSC, another potential signaling pathway between the N-DRC and I1 dynein through the T/TH complex.

In summary, we identified FAP43 (FAP244) and FAP44 as subunits of the heterodimeric T/TH complex that is an important regulator of I1 dynein and a highly inter-

connected “missing link” in the CPC-RS-I1 signaling pathway that regulates ciliary motility. The T/TH complex is highly conserved in eukaryotes, and defects of the complex may cause human ciliopathies. Indeed, a recent whole-exome sequencing study of human male infertility patients with multiple morphological abnormalities of the flagella (MMAF) showed that mutations in human FAP43 or FAP44 causes structural sperm defects, ciliary abnormalities, and impaired sperm motility (Tang *et al.*, 2017).

MATERIALS AND METHODS

Strains and culture

The strains used in this study (Supplemental Table S2), including *Tetrahymena thermophila* wild type (obtained from the *Tetrahymena* Stock Center, Cornell University, Ithaca, NY), generation of the *Tetrahymena fap43* genomic knockout mutants, as well as source and

genotyping of *Chlamydomonas reinhardtii* wild type and *fap44*, *fap43*, and *fap244* mutants (generated by the CLiP) (Zhang *et al.*, 2014; Li *et al.*, 2016) were described in detail in Urbanska *et al.* (2018).

Chlamydomonas cells were maintained on solid Tris-acetate-phosphate (TAP) medium and cultured in liquid TAP growth medium under 12:12 light:dark regime at 23°C with filtered air bubbling into the growing culture. *Tetrahymena* strains were maintained in SPP solution (2% protease peptone; 0.1% yeast extract; 0.2% glucose; penicillin G 100 U/ml; streptomycin 100 µg/ml; amphotericin B 0.25 µg/ml) and cultured in modified SPP medium (1% protease peptone; 0.1% yeast extract; 0.2% glucose; 0.003% ferric EDTA sodium salt; penicillin G 100 U/ml; streptomycin 100 µg/ml; amphotericin B 0.25 µg/ml). Cultivation of *Tetrahymena* strains were carried out at RT (25°C) with shaking in flasks at a speed of 60 rpm.

For the BCCP-gold labeling experiments, we combined two methods (BCCP-tag as reported in Oda and Kikkawa, 2013); smaller EM visible labeling protocols as developed by Song *et al.* (2015). The generation of *Tetrahymena* cells expressing BCCP-tagged proteins was described in detail in Urbanska *et al.* (2018). Briefly, to obtain *Tetrahymena* cells expressing either FAP43 or FAP44 with a C-terminal BCCP-tag under the control of their native promoter in the native *locus*, the tag coding region from pFAP43-3HA and pFAP44-2V5 native *locus* expression plasmids was replaced by a *Tetrahymena* BCCP coding region (Edamatsu, 2014) preceded by a 27 nucleotides linker encoding GSGGGS-GTG amino acid residues and single HA-tag. The obtained transgene was used to transform the CU428 wild-type *Tetrahymena* strain. Transformants were selected on SPP medium supplied with 100 µg/ml paromomycin and 1 µg/ml CdCl₂ and assorted as described (Urbanska *et al.*, 2018).

Axoneme preparation

Cilia and axonemes from *Tetrahymena* wild-type and *fap43* knock-out were isolated as previous described (Wloga *et al.*, 2008). Briefly, cilia pellets were resuspended in cold HMEEK buffer (30 mM HEPES, 25 mM KCl, 5 mM MgSO₄, 0.1 mM EDTA, and 0.2 mM ethylene-bis(oxyethylenenitrilo)tetraacetic acid) and demembrated by adding 1% Igepal CA 630 (Sigma-Aldrich) to the solution with gentle rotation for 20 min at 4°C. Axonemes were collected by centrifugation at 10,000 × *g* for 10 min. Preparation of *Chlamydomonas* axonemes were followed previously described protocols (Song *et al.*, 2015). Axonemal samples for both *Tetrahymena* and *Chlamydomonas* strains were either freshly used for cryo-ET purpose or stored at -80°C for biochemical experiments.

For cryo-ET sample preparation, freshly isolated axonemes (resuspended in HMEEK buffer) (*Tetrahymena* wild-type and *fap43* knockout strains; *Chlamydomonas* wild-type, *fap44*, *fap43*, *fap244*, and *ida2-7* strains) were plunge-frozen on glow-discharged (for 30 s at -35 mA) copper R2/2 holey carbon grids (Quantifoil Micro Tools GmbH, Jena, Germany) using a homemade plunge-freezer. In brief, 3 µl of the axonemal sample was applied to the grid and gently mixed with 1 µl of 10-times-concentrated, BSA-coated 10-nm gold solution (Iancu *et al.*, 2007). After ~2.0 s of backside blotting with Whatman filter paper, the grid was plunged into liquid ethane. Grids were stored in liquid nitrogen until used.

For BCCP labeling samples, axonemes isolated from *Tetrahymena* FAP43BCCP and FAP44BCCP cells were resuspended in 200 µl of HMEEK buffer. After 5 µl of 80 µg/ml 1.4-nm-sized streptavidin nanogold particles (Nanoprobes) was added, the solution was incubated for 4 h at 4°C. Control samples without added streptavidin nanogold particles were prepared at the same time. The axonemes were then washed by adding 800 µl of HMEEK buffer and

collected by centrifugation at 10,000 × *g* for 60 s. Cryosample preparation was carried out using the procedures described above.

Gel electrophoresis and immunoblotting

For SDS-PAGE, 20 µg of axonemal protein was separated on a 4–12% gradient SDS-polyacrylamide gel. For the 2DE experiment, 50 µg of axonemal protein was first separated on 7-cm immobilized pH 3–10 nonlinear gradient dry strips (GE Healthcare) and then separated on a 10% SDS-polyacrylamide gel. For immunoblotting, axonemal or ciliary proteins separated by SDS-PAGE or 2DE were transferred to a polyvinylidene difluoride membrane (Bio-Rad). The membrane was first incubated with 5% nonfat milk in TBST (Tris, 50 mM; NaCl, 150 mM; Tween-20, 0.1%; pH 7.5) for 1 h at RT and then with primary antibody overnight. Horseradish peroxidase-conjugated secondary antibody and a Clarity Western ECL substrate kit (Bio-Rad) was used to detect immune-reactive bands, which were visualized by use of the ChemiDoc™ Touch Imaging System (Bio-Rad). Primary antibodies used were as follows: anti-IC138 (rabbit; 1:10,000 dilution; Hendrickson *et al.*, 2004), anti-CK1 (rabbit; Gokhale *et al.*, 2009), anti-PP2A (B-subunit) (rabbit; 1:500 dilution; Elam *et al.*, 2011), and anti-IC2 (mouse; 1:10,000 dilution; Sigma-Aldrich). Immunoblots for both 2D and SDS-PAGE gels were replicated three times. Western blot signals of PP2A and CK1 were normalized to that of IC2 in Image Lab software (Bio-Rad).

LC-MS/MS

Axonemal samples (40 µg) were separated by SDS-PAGE on 4–12% gradient SDS-polyacrylamide gels. Samples were run into the gel for 3.0 mm, and the gels were stained with Coomassie brilliant blue. For each strain, the gel was cut into four slices, and each slice was further excised into 1-mm cubic pieces. Trypsin digestion and peptides identification were performed at the proteomics core facilities of Harvard University (for strains: *Tetrahymena* wild type and *fap43* knockout mutant; *Chlamydomonas* wild type and *fap44* mutant) or UT Southwestern Medical Center (for strains: *Chlamydomonas* wild type and *fap43*, *fap244*, *pf9-3* mutants). Identification of candidate components of the T/TH complex were based on mass spectrometry and the criterion that zero peptides were detected for the candidate protein in the T/TH-lacking mutant, whereas at least 10 unique peptides of the protein were detected in the wild-type sample. The ratio of the number of unique peptides from each tested protein from the *fap43* mutant to that from WT and from the *fap244* mutant to that of the WT (Supplemental Table S1) were calculated from the MIC Sin value (Trudgian *et al.*, 2011).

Phylogenetic analysis

Amino acid sequences of 53 T/TH proteins were extracted from UniProt (www.uniprot.org). Multiple sequence alignments were performed with Clustal X 2.0 (Larkin *et al.*, 2007). The maximum likelihood tree was constructed using MEGA6 (Tamura *et al.*, 2013)

Cryo-ET

Grids with frozen axonemes were imaged using a Tecnai F30 (ThermoFisher/FEI, Hillsboro, OR; used for all samples unless otherwise noted) or a Titan Krios transmission electron microscope (ThermoFisher/FEI; used only for samples from *C.r. fap244* and *C.r.* wild-type Volta-Phase-Plate data) both operated at 300 kV. Tilt series (from -60° to 60° tilt with 1.5–2.5° tilting increments) were recorded with a 2k × 2k charge-coupled device camera (Gatan, Pleasanton, CA) on the Tecnai F30 or a 4k × 4k K2 direct detection camera (Gatan) on the Titan Krios. Counting mode of the K2 camera was used and for each tilt image 15 frames (0.4-s exposure time for each frame) were

recorded. Both cameras were placed behind a postcolumn energy filter (Gatan) that was operated in zero-loss mode (20-eV slit width). Data acquisition was performed using the microscope control software SerialEM (Mastronarde, 2005) in low-dose mode, and the total electron dose per tilt series was limited to $\sim 100 \text{ e}/\text{\AA}^2$. A magnification of 13,500 (pixel size 1 nm) and defocus of $-8 \mu\text{m}$ were applied for the data collected on the Tecnai F30 (with charge-coupled device camera). A magnification of 26,000 (pixel size of 0.5 nm) and in-focus setting with a Volta-Phase-Plate (Danev *et al.*, 2014) were used for the data collected on the Titan Krios.

Image processing

The frames of each tilt series image collected on a K2 camera were aligned and then merged using the script extracted from the IMOD software package (Kremer *et al.*, 1996) to generate the final tilt serial data set. Tilt serial images were aligned using the 10-nm gold as fiducial markers using IMOD software (Kremer *et al.*, 1996). Tomogram reconstruction was done by weighted back-projection method in IMOD, and the axonemal 96-nm-long repeats were picked from the raw tomograms. Subtomogram averaging was performed using the PEET software (Nicastro *et al.*, 2006). The UCSF Chimera package software (Pettersen *et al.*, 2004) was used to visualize the three-dimensional structure of the averaged 96-nm-long axonemal repeats by isosurface rendering. Classification analyses were carried out with a principal component analysis clustering method (Heumann *et al.*, 2011). Supplemental Table S2 summarizes the number of tomograms and axonemal repeats as well as estimated resolution for each strain used in this study. Resolution estimation was measured at the base of RS1 with a criterion of 0.5 using the Fourier shell correlation method.

ACKNOWLEDGMENTS

We thank Winfield S. Sale (Emory University) for generously providing antibodies against IC138, CK1, and PP2A (B sub). We also thank Xu Chen (Brandeis University) and Zhenguo Chen (UT Southwestern Medical Center) for management of the electron microscope facilities and training. The UT Southwestern Cryo-Electron Microscopy Facility is funded in part by CPRIT Core Facility Support Award RP170644. For LC-MS/MS analysis, we thank the proteomics core facilities at Harvard University and UT Southwestern Medical Center. We also thank Xiaowei Zhao (UT Southwestern Medical Center) for assisting with tomogram reconstruction. We are grateful to Jerry Brown and Long Gui for critical reading of the manuscript. This study was supported by the following grants: National Institutes of Health R01GM083122 to D.N., Polish Ministry of Science and Higher Education Grant No. N301706640 and National Science Centre, Poland, Grant 2014/14/M/NZ3/00511 (Harmonia 6) to D.W., and National Science Centre, Poland, Grant 2014/13/N/NZ3/04612 (Preludium 7) to P.U.

REFERENCES

Afzelius BA (2004). Cilia-related diseases. *J Pathol* 204, 470–477.
 Bower R, VanderWaal K, O'Toole E, Fox L, Perrone C, Mueller J, Wirschell M, Kamiya R, Sale WS, Porter ME (2009). IC138 defines a subdomain at the base of the I1 dynein that regulates microtubule sliding and flagellar motility. *Mol Biol Cell* 20, 3055–3063.
 Danev R, Buijsse B, Khoshouei M, Plitzko JM, Baumeister W (2014). Volta potential phase plate for in-focus phase contrast transmission electron microscopy. *Proc Natl Acad Sci USA* 111, 15635–15640.
 Dymek EE, Heuser T, Nicastro D, Smith EF (2011). The CSC is required for complete radial spoke assembly and wild-type ciliary motility. *Mol Biol Cell* 22, 2520–2531.

Dymek EE, Smith EF (2007). A conserved CaM- and radial spoke-associated complex mediates regulation of flagellar dynein activity. *J Cell Biol* 179, 515–526.
 Edamatsu M (2014). Identification of biotin carboxyl carrier protein in *Tetrahymena* and its application in in vitro motility systems of outer arm dynein. *J Microbiol Methods* 105, 150–154.
 Elam CA, Wirschell M, Yamamoto R, Fox LA, York K, Kamiya R, Dutcher SK, Sale WS (2011). An axonemal PP2A B-subunit is required for PP2A localization and flagellar motility. *Cytoskeleton (Hoboken)* 68, 363–372.
 Fliegauf M, Benzing T, Omran H (2007). When cilia go bad: cilia defects and ciliopathies. *Nat Rev Mol Cell Biol* 8, 880–893.
 Gokhale A, Wirschell M, Sale WS (2009). Regulation of dynein-driven microtubule sliding by the axonemal protein kinase CK1 in *Chlamydomonas* flagella. *J Cell Biol* 186, 817–824.
 Goodenough U, Heuser J (1985). Outer and inner dynein arms of cilia and flagella. *Cell* 41, 341–342.
 Habermacher G, Sale WS (1997). Regulation of flagellar dynein by phosphorylation of a 138-kD inner arm dynein intermediate chain. *J Cell Biol* 136, 167–176.
 Hendrickson TW, Perrone CA, Griffin P, Wuichet K, Mueller J, Yang P, Porter ME, Sale WS (2004). IC138 is a WD-repeat dynein intermediate chain required for light chain assembly and regulation of flagellar bending. *Mol Biol Cell* 15, 5431–5442.
 Heumann JM, Hoenger A, Mastronarde DN (2011). Clustering and variance maps for cryo-electron tomography using wedge-masked differences. *J Struct Biol* 175, 288–299.
 Heuser T, Barber CF, Lin J, Krell J, Rebesco M, Porter ME, Nicastro D (2012a). Cryoelectron tomography reveals doublet-specific structures and unique interactions in the I1 dynein. *Proc Natl Acad Sci USA* 109, E2067–E2076.
 Heuser T, Dymek EE, Lin J, Smith EF, Nicastro D (2012b). The CSC connects three major axonemal complexes involved in dynein regulation. *Mol Biol Cell* 23, 3143–3155.
 Iancu CV, Tivol WF, Schooler JB, Dias DP, Henderson GP, Murphy GE, Wright ER, Li Z, Yu Z, Briegel A, *et al.* (2007). Electron cryotomography sample preparation using the Vitrobot. *Nat Protoc* 1, 2813–2819.
 Kamiya R, Yagi T (2014). Functional diversity of axonemal dyneins as assessed by in vitro and in vivo motility assays of *Chlamydomonas* mutants. *Zool Sci* 31, 633–644.
 Kikkawa M (2013). Big steps toward understanding dynein. *J Cell Biol* 202, 15–23.
 King SJ, Dutcher SK (1997). Phosphoregulation of an inner dynein arm complex in *Chlamydomonas reinhardtii* is altered in phototactic mutant strains. *J Cell Biol* 136, 177–191.
 Kremer JR, Mastronarde DN, McIntosh JR (1996). Computer visualization of three-dimensional image data using IMOD. *J Struct Biol* 116, 71–76.
 Larkin MA, Blackshields G, Brown NP, Chenna R, McGettigan PA, McWilliam H, Valentin F, Wallace IM, Wilm A, Lopez R, *et al.* (2007). Clustal W and Clustal X version 2.0. *Bioinformatics* 23, 2947–2948.
 Li X, Zhang R, Patena W, Gang SS, Blum SR, Ivanova N, Yue R, Robertson JM, Lefebvre PA, Fitz-Gibbon ST, *et al.* (2016). An indexed, mapped mutant library enables reverse genetics studies of biological processes in *Chlamydomonas reinhardtii*. *Plant Cell* 28, 367–387.
 Lin J, Heuser T, Song K, Fu X, Nicastro D (2012). One of the nine doublet microtubules of eukaryotic flagella exhibits unique and partially conserved structures. *PLoS One* 7, e46494.
 Lin J, Nicastro D (2018). Asymmetric distribution and spatial switching of dynein activity generates ciliary motility. *Science*, DOI: 10.1126/science.aar1968.
 Lin J, Yin W, Smith MC, Song K, Leigh MW, Zariwala MA, Knowles MR, Ostrowski LE, Nicastro D (2014). Cryo-electron tomography reveals ciliary defects underlying human RSPH1 primary ciliary dyskinesia. *Nat Commun* 5, 5727.
 Mastronarde DN (2005). Automated electron microscope tomography using robust prediction of specimen movements. *J Struct Biol* 152, 36–51.
 Mitchison TJ, Mitchison HM (2010). Cell biology: how cilia beat. *Nature* 463, 308–309.
 Myster SH, Knott JA, O'Toole E, Porter ME (1997). The *Chlamydomonas* Dhc1 gene encodes a dynein heavy chain subunit required for assembly of the I1 inner arm complex. *Mol Biol Cell* 8, 607–620.
 Myster SH, Knott JA, Wysocki KM, O'Toole E, Porter ME (1999). Domains in the 1 α dynein heavy chain required for inner arm assembly and flagellar motility in *Chlamydomonas*. *J Cell Biol* 146, 801–818.
 Nicastro D, Schwartz C, Pierson J, Gaudette R, Porter ME, McIntosh JR (2006). The molecular architecture of axonemes revealed by cryoelectron tomography. *Science* 313, 944–948.

- Oda T, Kikkawa M (2013). Novel structural labeling method using cryo-electron tomography and biotin-streptavidin system. *J Struct Biol* 183, 305–311.
- Pazour GJ, Agrin N, Leszyk J, Witman GB (2005). Proteomic analysis of a eukaryotic cilium. *J Cell Biol* 170, 103–113.
- Pettersen EF, Goddard TD, Huang CC, Couch GS, Greenblatt DM, Meng EC, Ferrin TE (2004). UCSF Chimera—a visualization system for exploratory research and analysis. *J Comput Chem* 25, 1605–1612.
- Piperno G, Mead K, LeDizet M, Moscatelli A (1994). Mutations in the “dynein regulatory complex” alter the ATP-insensitive binding sites for inner arm dyneins in *Chlamydomonas* axonemes. *J Cell Biol* 125, 1109–1117.
- Porter ME, Sale WS (2000). The 9 + 2 axoneme anchors multiple inner arm dyneins and a network of kinases and phosphatases that control motility. *J Cell Biol* 151, F37–F42.
- Smith EF (2002). Regulation of flagellar dynein by the axonemal central apparatus. *Cytoskeleton* 52, 33–42.
- Smith EF, Lefebvre PA (1997). The role of central apparatus components in flagellar motility and microtubule assembly. *Cell Motil Cytoskeleton* 38, 1–8.
- Smith EF, Sale WS (1992). Regulation of dynein-driven microtubule sliding by the radial spokes in flagella. *Science* 257, 1557–1559.
- Song K, Awata J, Tritschler D, Bower R, Witman GB, Porter ME, Nicastro D (2015). In situ localization of N and C termini of subunits of the flagellar nexin-dynein regulatory complex (N-DRC) using SNAP tag and cryo-electron tomography. *J Biol Chem* 290, 5341–5353.
- Tamura K, Stecher G, Peterson D, Filipinski A, Kumar S (2013). MEGA6: molecular evolutionary genetics analysis version 6.0. *Mol Biol Evol* 30, 2725–2729.
- Tang S, Wang X, Li W, Yang X, Li Z, Liu W, Li C, Zhu Z, Wang L, Wang J, et al. (2017). Biallelic mutations in *CFAP43* and *CFAP44* cause male infertility with multiple morphological abnormalities of the sperm flagella. *Am J Hum Genet* 100, 854–864.
- Toba S, Fox LA, Sakakibara H, Porter ME, Oiwa K, Sale WS (2011). Distinct roles of 1alpha and 1beta heavy chains of the inner arm dynein I1 of *Chlamydomonas* flagella. *Mol Biol Cell* 22, 342–353.
- Trudgian DC, Ridlova G, Fischer R, Mackeen MM, Ternette N, Acuto O, Kessler BM, Thomas B (2011). Comparative evaluation of label-free SINQ normalized spectral index quantitation in the central proteomics facilities pipeline. *Proteomics* 11, 2790–2797.
- Urbanska P, Joachimiak E, Bazan R, Fu G, Poprzeczko M, Fabczak H, Nicastro D, Wloga D (2018). Ciliary proteins Fap43 and Fap44 interact with each other and are essential for proper cilia and flagella beating. *Cell Mol Life Sci*, DOI: 10.1007/s00018-018-2819-7 (in press).
- Urbanska P, Song K, Joachimiak E, Krzemien-Ojak L, Koprowski P, Hennessey T, Jerka-Dziadosz M, Fabczak H, Gaertig J, Nicastro D, et al. (2015). The CSC proteins FAP61 and FAP251 build the basal substructures of radial spoke 3 in cilia. *Mol Biol Cell* 26, 1463–1475.
- VanderWaal KE, Yamamoto R, Wakabayashi K-I, Fox L, Kamiya R, Dutcher SK, Bayly PV, Sale WS, Porter ME (2011). bop5 Mutations reveal new roles for the IC138 phosphoprotein in the regulation of flagellar motility and asymmetric waveforms. *Mol Biol Cell* 22, 2862–2874.
- Viswanadha R, Sale WS, Porter ME (2017). Ciliary motility: regulation of axonemal dynein motors. *Cold Spring Harb Perspect Biol* 9, a018325.
- Wirschell M, Hendrickson T, Sale WS (2007). Keeping an eye on I1: I1 dynein as a model for flagellar dynein assembly and regulation. *Cell Motil Cytoskeleton* 64, 569–579.
- Wirschell M, Yamamoto R, Alford L, Gokhale A, Gaillard A, Sale WS (2011). Regulation of ciliary motility: conserved protein kinases and phosphatases are targeted and anchored in the ciliary axoneme. *Arch Biochem Biophys* 510, 93–100.
- Wirschell M, Yang C, Yang P, Fox L, Yanagisawa H-A, Kamiya R, Witman GB, Porter ME, Sale WS (2009). IC97 is a novel intermediate chain of I1 dynein that interacts with tubulin and regulates interdoublet sliding. *Mol Biol Cell* 20, 3044–3054.
- Witman GB, Plummer J, Sander G (1978). *Chlamydomonas* flagellar mutants lacking radial spokes and central tubules. Structure, composition, and function of specific axonemal components. *J Cell Biol* 76, 729–747.
- Wloga D, Rogowski K, Sharma N, Van Dijk J, Janke C, Edde B, Bre MH, Levilliers N, Redeker V, Duan J, et al. (2008). Glutamylation on alpha-tubulin is not essential but affects the assembly and functions of a subset of microtubules in *Tetrahymena thermophila*. *Eukaryotic Cell* 7, 1362–1372.
- Yamamoto R, Song K, Yanagisawa H-A, Fox L, Yagi T, Wirschell M, Hirono M, Kamiya R, Nicastro D, Sale WS (2013). The MIA complex is a conserved and novel dynein regulator essential for normal ciliary motility. *J Cell Biol* 201, 263–278.
- Yang P, Sale WS (2000). Casein kinase I is anchored on axonemal doublet microtubules and regulates flagellar dynein phosphorylation and activity. *J Biol Chem* 275, 18905–18912.
- Zhang R, Patena W, Armbruster U, Gang SS, Blum SR, Jonikas MC (2014). High-throughput genotyping of green algal mutants reveals random distribution of mutagenic insertion sites and endonucleolytic cleavage of transforming DNA. *Plant Cell* 26, 1398–1409.